von Karman Institute for Fluid Dynamics

STO-AVT-VKI Lecture Series 2016/17 – AVT 289

Lecture Series on

MULTIPHYSICS PHENOMENA ANALYSIS ON BOUNDARY LAYER STABILITY IN HYPERSONIC REGIME

September 18-20, 2017

TRANSITIONAL SHOCK WAVE BOUNDARY LAYER INTERACTION

P. Dupont
IUSTI, Aix Marseille University, CNRS, France

Transitional shock wave boundary layer interaction

Pierre Dupont
IUSTI
Aix Marseille University, CNRS UMR 7343
5 rue Enrico Fermi
Marseille, 13013
France

pierre.dupont@univ-amu.fr

ABSTRACT

The spatial development of a transitional Oblique Shock Wave Interaction at Mach 1.68 is documented thanks to high resolution Laser Doppler Anemometer (LDA) and Hot Wire Anemometer (HWA) measurements. The amplifications of the velocity fluctuations along the transitional separated shear layer is found to follow an exponential growing. The time properties of these unsteadiness are characterized with external hot wire measurements and the transition to turbulence of the separated shear layer is described. It is shown that the interaction tend to amplify preferentially characteristic frequencies. Low frequency unsteadiness of the interaction is observed and are compared with similar turbulent interactions.

Contents

1.0 INTRODUCTION

Since its first appearance in the 40s, shock-wave boundary layer interactions (SWBLI) have been widely studied numerically and experimentally, both with upstream laminar or turbulent boundary layer. SWBLI appear

in supersonic engines, such as at the extrados of a supersonic air-plane, in supersonic air intakes or in over-expanded nozzles. Depending on whether the boundary layer is separated or not, the upstream state is laminar or turbulent, the topology of SWBLI can be very different.
A large part of SWBLI studies considered a turbulent boundary layer, and were realized using several geometric configurations (see previous lecture *Unsteadiness in turbulent shock wave boundary layer interaction*).
Compared to turbulent SWBLI, supersonic configurations with upstream laminar conditions have been less investigated ([1–5]). Nevertheless, they have recently gained interest since aeronautical industries are confronted to the challenging reduction of air-plane impact on the environment. In this context, reduction of greenhouse gaze can be achieved, in particular, by reducing air-plane drag. A solution may consist of the use of laminar profile at high altitude where favorables conditions (low Reynolds numbers) allow the boundary layer to stay laminar a long distance downstream from the leading edge. The laminar boundary layer in the first part of the airfoil ensures a significant drag reduction with regards to the case where the boundary is turbulent, since turbulent boundary layer is known to produce more drag than laminar boundary layer. Unfortunately, the laminar boundary layer can separate easier than a turbulent boundary layer, when it sustains an adverse pressure gradient, and this causes worsening of aerodynamic performances. Moreover, transition to turbulence is very sensitive to pressure gradient and may occurs along the interaction.
Intensives researches on laminar airfoils on which the boundary layer remains laminar down to the shock on the upper part of the wing have been carried out. Recently, the European program TFAST (Transition Location Effect on Shock Wave Boundary Layer Interaction), considered such transitional interactions for various cases (flat plate, airfoil and turbo-machinery configurations). As for the turbulent SWBLI, the mean properties of the flow are quite well described. The main differences, in respect with the turbulent configurations, are the extreme sensitivity to the separation and a dramatic increase of the aspect ratio of the interactions.
When unsteady aspects are considered, far less informations, experimental as well as numerical, are available. For example, in turbulent SWBLI, several studies have confirmed the existence of low frequency unsteadiness of the separated SWBLI, with a characteristic frequency of two order of magnitude lower than the characteristics frequencies of the incoming boundary layer. For the laminar upstream conditions different cases have been observed [6] depending on the location of the transition to the turbulence:

- for fully laminar interactions (the transition is located downstream from the reattachment of the flow), no evidence of unsteadiness are reported
- for transitional interaction, the transitions occurs inside the interaction and promotes the reattachment of the flow. In this case, low frequency unsteadiness can be observed from schlieren visualizations, depending on the intensity of the interaction.

Such behaviour has been recently confirmed from experimental and numerical results obtained during the TFAST program [7–11]).
In this lecture, the particular case of a Mach 1.68 laminar boundary layer interaction with an incident oblique shock wave is considered. As for the turbulent SWBLI, we will detail the properties of the mean fields, then the unsteady aspects will be addressed. Compared to a turbulent SWBLI, level and spectral characteristic of the upstream perturbations are completely modified, as well as the aspect ratio of the separated bubble. Therefore, these new results could contribute to validate the different models developed for the turbulent cases.
The experimental set-up will be presented in section 2.0. The mean flow properties will be presented in part 3.0, with the necessary improvements of the Hot Wire (HW) and Laser Doppler Anemometer (LDA). Indeed, the experimental conditions are particularly difficult for time space resolved measurements and necessitate specific systems. Then, the time scales developing along the interaction will be presented in section 4.0. Finally a

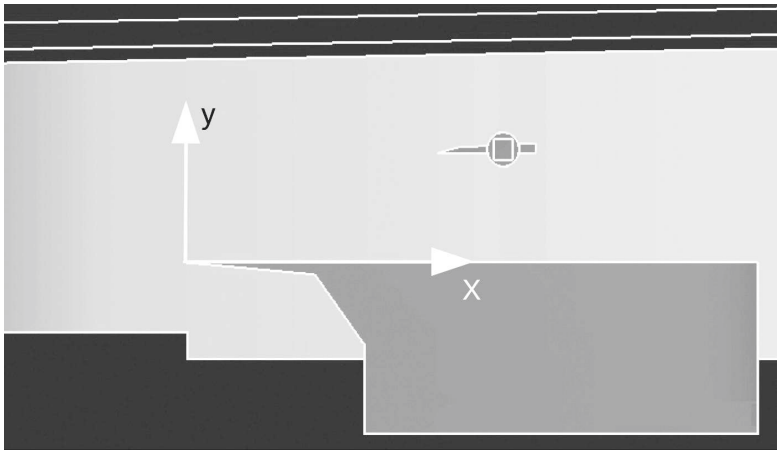

Figure 1: Test section with model

discussion about the transitional mechanism along the interaction is presented section 5.0. the resulting time scales are compared with other transitional cases and with separated turbulent SWBLI.

2.0 EXPERIMENTAL SET-UP

Experiments are carried out in the hypo-turbulent supersonic wind tunnel of the IUSTI laboratory, at the Aix-Marseille University, France. This is a continuous facility with a closed-loop circuit. The nominal Mach number of the test section is $M = 1.68$, and the total pressure was set from 0.4×10^5Pa to 0.8×10^5Pa. The turbulence intensity of the pressure fluctuations in the potential flow are as low as 0.4% at this stagnation pressure. The unitary Reynolds number is $Re_u = 5.7 \times 10^6$ for total pressure of 0.4×10^5Pa. The reflection of an oblique shock wave on a laminar supersonic boundary layer developing over a flat plate is considered. The model is composed of a flat plate of 175mm long. A sharp-edged shock generator is installed at 72mm downstream of the leading edge of the flat plate and at 30mm distance from the wall of the plate. The shock generator and the flat plate spans are as large as the wind tunnel test section. The origin of the abscissa X is taken at the leading edge of the flat plate. The flow deviation θ can be varied without blockage effects from $2°$ to $6°$. To limit blockage effects, the shock generator is directly housing into plexiglas windows, and a cavity is made underneath the plate. A sketch of the experimental set-up is shown Figure 1.

The impingement location of the incident shock wave X_{imp} is at 107.3mm from the leading edge. The upstream influence of the interaction X_0 has been defined as the extrapolation down to the wall of the inflection point of the pressure rise across the compression waves (derived from Pitot measurements at 5mm from the wall, see part 3.0). This position can be seen as the mean position of the separation point. The non-dimensional longitudinal coordinate is $X^* = (X - X_{imp})/L$. The position of the incident shock at the wall is then $X^* = 0$ and the compression waves are centered around $X^* = -1$.

During the project TFAST, it was found that it was not possible to obtain a reasonable seeding to achieve instantaneous Particle Image Velocity measurements: only mean velocity fields were resolved [12]. Therefore, in order to derive unsteady measurements, the flow was documented using Hot Wire Anemometer and Laser Doppler Anemometer. The Hot Wire Anemometer was operated in constant temperature configuration (CTA) from *Dantec Dynamics* (*Streamline system*). The wire length is about $1mm$ while its diameter is of $5\mu m$. It is operated at an overheat ratio of $a_w = 0.8$: for such an overheat ratio, the anemometer is mainly sensitive to

Table 1: LDA characteritics

Laser emission

λ [nm]	Beam $\varnothing$ [nm]	Beam spacing [mm]	Beam expander ratio	F Bragg cell[MHz]
514	2.25	19	1.98	40

Measurement volume

length [nm]	$\varnothing$ [μm]	Fringe spacing [μm]	F_{max} [MHz]	incense smoke $\varnothing$ [nm]
1.9	75	6.70	110	500

the momentum fluctuations. The anemometer bridge is set in symmetric configuration. Its settings are made through the *Dantec Dynamics* software *Streamware*, in the outer flow. The cut-off frequency was estimated from the response of the anemometer to square wave signals for each stagnation pressure, since the bandwidth frequency of the anemometer depends on the unitary Reynolds number. The bandwidth varies from 80 to $130kHz$ for unitary Reynolds numbers varying between $5.6 \times 10^6 m^{-1}$ ($P_t = 0.4atm$) and $12 \times 10^6 m^{-1}$ ($P_t = 0.8atm$). A low pass filter with a cut-off frequency of $100kHz$ is applied. The measured analog signal is acquired using a 14bit fast digital converter *NI6133* from National Instrument. For each acquisition, two millions points have been acquired at a sampling frequency of 400kHz (five seconds of acquisition).
Finally, Laser Doppler Anemometer (LDA) is used to measure flow velocity and turbulence intensity inside of the boundary layer. We used an Argon-ion laser from *Spectra-Physics (*$6W$*,* $Stabilite$ 2017*)*. Only the most energetic wave length ($\lambda = 514.5nm$) is used, to measure the longitudinal component of the velocity. The emitted beam is split into 2 parallels beams of a diameter of $2.25mm$ through a FiberFlow system from *Dantec Dynamics*. A Bragg Cell imposes a shifting frequency of $40MHz$ at one of the beam, allowing the system to resolve negative velocity. A beam-spacer is used to adjust the distance between the two beams to $19.3mm$. A beam expander with 1.98 ratio and a $50cm$ converging lens are used, leading to a measurement volume of $75\mu m$ diameter and $1.9mm$ length. The receptive head is backward positioned, off-axis. The off-axis angle is about $25°$, in order to receive the maximum light emanating from particles in the backward configuration and then to optimize the signal to noise ratio. We use particles of incense smoke whose average size is $500nm$ to seed the flow [13]. Particles are seeded through a seeding cane placed at the end of the plenum chamber, on the wind tunnel axis. The seeding system is adjustable vertically in order to seed the interaction zone. The mains LDA characteristics are summarize on Table 1.

3.0 MEAN FLOW PROPERTIES

3.1 Laminar boundary layer

The boundary layer which is developing along the flat plate has been controlled to be laminar [14]. For a theoretical laminar boundary, velocity profiles are self-similar: $U/Ue = f(y\sqrt{Re_u/x})$, where Re_u is the unitary Reynolds number. Indeed, the boundary layer thickness evolves as :$\delta \propto \sqrt{x/Re_u}$. Figure 2 represents the mean velocity profiles obtained from LDA measurements, for positions ranging from 80mm to 160mm and for stagnation pressure from 0.4atm to 0.8atm, it means for Reynolds numbers Re_x from $0,448 \times 10^6$ to 0.919×10^6. As seen on the figure, boundary layer profiles are in a good agreement with the compressible laminar profile obtained from StarCCM+ computation.

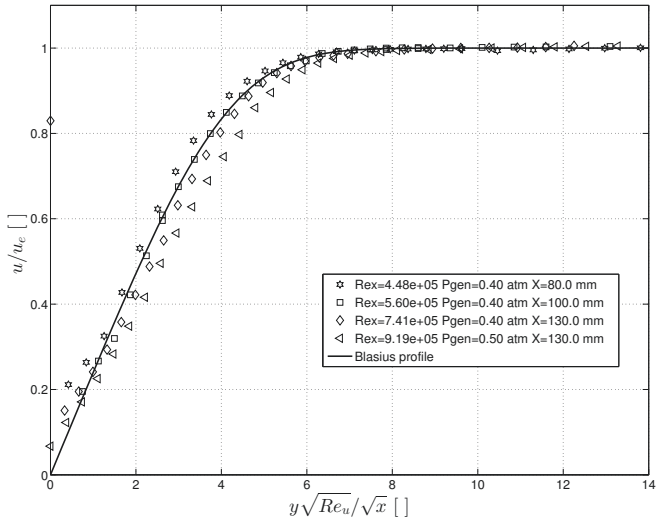

Figure 2: Velocity profiles in normalized representation - LDA meaurements ($75m$)[14]

At the impingement shock location ($X = 107.3$), the undisturbed boundary layer thickness is $\delta_{imp} = 0.9$mm and the displacement thickness is $\delta^*_{imp} = 0.4$mm. At the mean separation location, the undisturbed boundary layer thickness is $\delta_0 = 0.7$mm and the displacement thickness is $\delta^*_0 = 0.3$mm. Hence, the boundary layer thickness dependency on the longitudinal position x and the unit Reynolds number Re_u is given by:

$$\delta = 6.67\frac{\sqrt{x}}{\sqrt{Re_u}}$$

The displacement thickness can be derived:

$$\delta_{1i} = \overline{\delta_{1i}}\frac{\sqrt{x}}{\sqrt{Re_u}} \tag{1}$$

with $\overline{\delta_{1i}} = 2374$. The momentum thickness can be expressed as:

$$\delta_{2i} = \overline{\delta_{2i}}\frac{\sqrt{x}}{\sqrt{Re_u}} \text{ avec } \overline{\delta_{2i}} = 908 \tag{2}$$

Finally, the form factor H can be derived from the relations 1 and 2:

$$H_i = \frac{\overline{\delta_{1i}}}{\overline{\delta_{2i}}} \simeq 2.61 \tag{3}$$

3.2 Improvements in metrology

The LDA probe volume diameter Φ used for results presented Figure 2 is 75μm, see Table 1. It has to be compared with the thickness of the boundary layer at the section X_0 which is as small as 700μm. Therefore,

the velocity gradient across the diameter of the probe volume cannot be neglected. Based on classical models to take into account the velocity gradient inside the probe volume [15], an analytical expression of the bias measurements was derived [16]. The apparent intensity of velocity fluctuations is then

$$\frac{u'}{U_e} = \frac{\Phi}{2\sqrt{3}} * \frac{1}{2}\left(\left|\frac{U_i - U_{i-1}}{y_i - y_{i-1}}\right| + \left|\frac{U_{i+1} - U_i}{y_{i+1} - y_i}\right|\right) \tag{4}$$

with subscript *i* designating the current position of the measurement volume and U_i the velocity at this position. Taking into account the electronic limitation of the electronic devices, a probe volume with a diameter of $38m$ was created. This new LDA set up is used to achieved measurement of the longitudinal velocity fluctuations along the interaction. It is clear that, whatever the LDA-set up, no significant unsteady measurements can be achieved in the laminar boundary layer: the expected levels are too small when compared with the artificial turbulence or the remaining noise. For the stations downstream from the separation point ($X^* > -1$), RMS values become significantly larger than the apparent turbulence and accurate measurements can be derived if the measurements are corrected from the artificial turbulence.
The hot wire probe is small enough ($5m$) to resolve accurate measurements. Nevertheless, any vibrations of the probe will create, as for the LDA, artificial fluctuations. Therefore a specific probe was designed to achieve measurements in the upstream laminar boundary layer. The probe was designed in such a way that it is possible to lean the probe against the wall, in order to avoid mechanical vibrations of the prongs. This probe has been used to characterize the unsteady scales in the upstream laminar boundary layer and to evaluate the transition location, observed for Reynolds number based on the longitudinal position X of about 3×10^6.
For the measurements along the interaction, downstream from the separation, the flow is decelerated, transonic effects are massive and reverse flow are occurring. Therefore, no HW measurements were achieved inside the shear layer. Only measurements outside the shear region, in the potential flow, has been carried out to measure the pressure perturbations radiated from the shear layer [17].

3.3 General flow organization

As mentioned in part 2.0, the shock generator is housing into the plexiglas windows. The mechanical constraints, when the flow is started up, preclude to achieve good quality schlieren pictures. An ombroscopy visualization of the interaction is shown figure 3(a): despite several optical aberrations, the global organization is clearly visible: the incident shock wave, the upstream influence with the thickening of the laminar boundary layer. However, the upstream compression wave are not visible. Quantitative characterization of the interaction has been derived from the pressure measurements along the interaction, performed at $5mm$ from the wall, are plotted on Figure 3(b). On this figure, a first smooth pressure rise corresponding to reflected compression waves can be observed. This area is followed by a pressure plateau, characteristic of separated interactions (Délery and Marvin [18]), which is ended by the incident oblique shock wave. We also see, downstream of the incident shock, a second plateau pressure and an expansion zone. The length of the interaction L, defined as the distance between X_0 and X_{imp}, is of 43.7mm.
The flow deviation at the separation point (θ_{sep}) can be derived, as well as the Mach numbers downstream from the compression waves (M_2) and from the incident shock (M_3). The associated sketch of the interaction is presented on Figure 4.
The classical Free Interaction Theory (Chapman et al. [6]) suggests that separation conditions (pressure, flow deviation) are independent from the imposed flow deviation (θ): this is clearly verified by the present measurements (see Figure 5). This theory gives also some evaluation of the pressure rise across the initial part of the

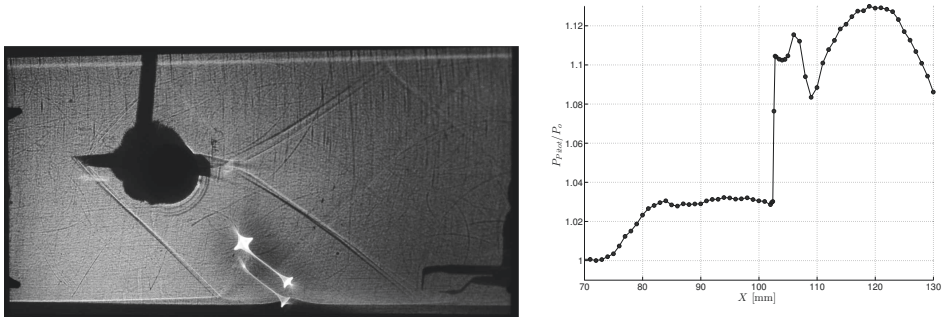

(a) (b)

Figure 3: Mean flow organization: (a) Ombroscopy; (b) Pitot profile along the interaction. Measurements at $y = 5mm$ from the wall; $P_o = 0.8atm$, $\theta = 6^\circ$

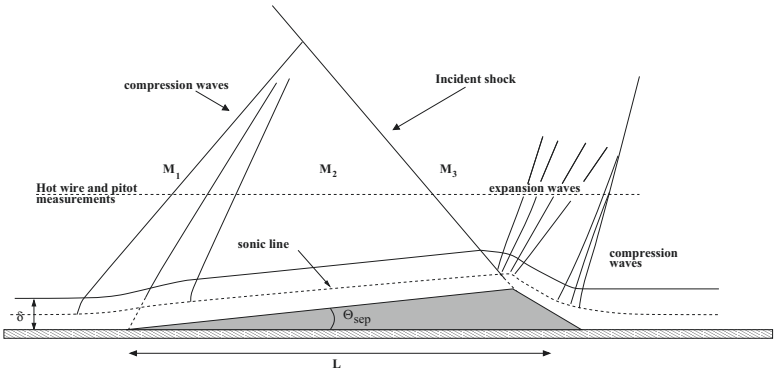

Figure 4: Sketch of a separated laminar boundary layer interaction

interaction, down to the plateau region. The plateau static pressure is given by:

$$\frac{p - p_0}{p_0} = \frac{1}{2}\gamma M_0^2 F \sqrt{\frac{2C_{f_0}}{(M_0^2 - 1)^{1/2}}} \tag{5}$$

where M_0, p_0 and C_{f_0} are the upstream conditions at the beginning of the pressure rise. F is a constant that depends on the nature the interaction. For laminar separations, it is found by means of experimental correlations to be equal to 1.5. The value of the constant F has been evaluated in our flow case, from the present Pitot measurements. We found a value of $F = 1.64$, corresponding to an error of 9% with respect to the constant given by Chapman [6]. Mean and turbulent longitudinal velocity profiles have been documented along the interaction (see Figure 6). The mean longitudinal velocity at several sections achieved with the $38\mu m$ probe volume LDA anemometer is reported Figure 6(a). It evolves gradually from a laminar, to inflectional profiles in the interaction region, then to fulfilled velocity profiles downstream from the reattachment point. In the initial interaction region, near wall points had very low data rate and measurements were not reliable. Superimposed on the figure, the line with circles represents the location of the 99% boundary layer thickness, and the line with triangles give a first approximation of the recirculation zone: it corresponds to the location of the first positive velocity measured. As already mentioned, in the first part of the recirculation zone, no - or very few- particles are present, and this line is located at the last position where measurements were possible. Its longitudinal

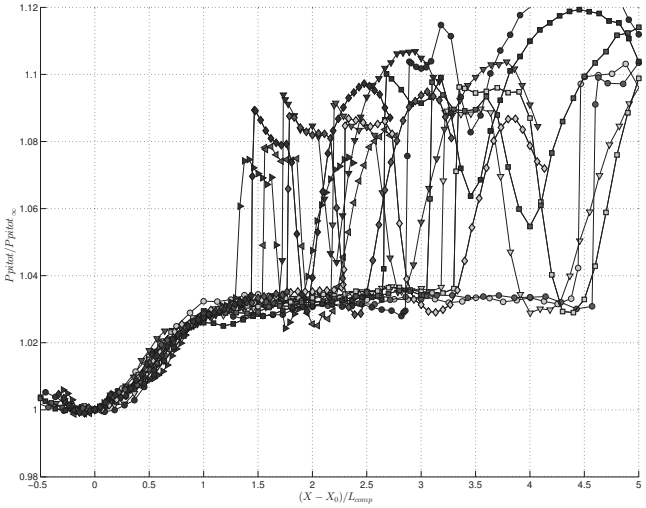

Figure 5: Profils longitudinaux de pression mesurs $y = 5mm$ de la paroi pour diverses pressions gnratrices et angles de gnrateur de choc

elevation can be considered as an approximation of the streamline corresponding to the no-seeded region. A clear dissymmetry of the interaction is observed on both sides of the apex (maximum elevation of the separated bubble), with a large upstream influence and, on the opposite, a reattachment in vicinity of the impingement location as reported by other TFAST's partners[7, 11, 12].
Downstream from the station $X^* = -0.18$, the turbulence intensity of velocity fluctuations is increasing dramatically (see figure 6(b)): it varies from about 1% of the external velocity U_e (which is the noise level of these LDA measurements) to a saturation level of about $0.17U_e$ near the incident shock impingement location. In the initial part of the interaction ($-1 < X^* < -0.5$), the amplitude of the velocity of fluctuations are too low to be resolved from the present LDA measurements. In the second part, the shear layer is seeded down to the wall and the mean recirculating region is clearly resolved by the LDA measurements. Flow is reattaching between the locations $X^* = 0$ and $X^* = 0.2$. The apex is found at $X^* = -0.2$ at $y = 1.3mm$. As the length of interaction is of $43.7mm$, this leads to a flow deviation at the separation point of about $\theta_{sep} = tan^{-1}(1.3/(0.8 * L)) \simeq 2.1°$. This compares accurately with prediction from classical Free interaction Theory (eq. 5).

4.0 TIME SCALES ALONG THE INTERACTION

LDA measurements provides new results on the velocity fluctuations inside the separated shear layer. Unfortunately, the data-rates were not high enough (typically around 1 to 5kHz) to resolve accurately their time properties. Therefore, hot wire measurements have been achieved in order to derive the Power Spectral Densities of the momentum fluctuations. As measurements inside the separated shear layer were of limited accuracy (probe vibrations, transonic effects, recirculating flows), we measured over the shear layer ($y = 5mm$) the radiated pressure perturbations ([19], pp25-32 et p125, [17], [20]). The measured intensity of voltage fluctuations along the interaction is compared to the longitudinal evolution of the maxima RMS velocity fluctuations derived from LDA measurements (see figure 7). On this figure, the location of the hot wire measurements were corrected from the angle of the characteristics for a Mach number of 1.68 to match with LDA measurement

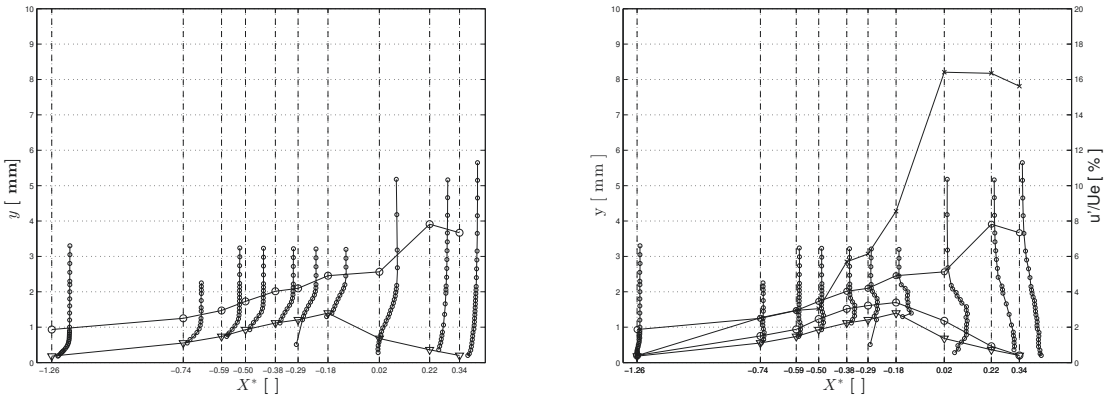

(a) (b)

Figure 6: Mean (a) and turbulent ??longitudinal velocity LDA measurements ($38\mu m$), $\theta = 5°$, $P_0 = 0.4atm$ longitudinal velocity LDA measurements along the interaction with the $38\mu m$ probe volume.

positions. Three different zones located upstream of the incident shock can be defined from the HW results:

- the *compression zone* ($-1.1 < X^* < -0.9$), with a bump of intensity, associated to the unsteady upstream compression waves
- the *initial part of the plateau zone* ($-0.9 < X^* < -0.5$), where values remain at a nearly constant level
- the *second part of the plateau zone* ($-0.5 < X^* < -0.2$) where a large increase of the turbulent intensity is observed.

Similar evolution are obtained for the LDA measurements, with a large increase of the velocity fluctuations in the second part of the interaction ($-0.5 < X^*$). As already mentioned, LDA measurements are not reliable for $X^* < -0.5$. This shows that the radiated fluctuations can be used to analyze the evolution of the unsteadiness along the separated shear layer. Therefore, HWA measurements are used to characterize the times scales developing along the interaction.

The pre-multiplied PSD are plotted along the interaction for the three different zones (see Figure 8). The Figure 8(a) highlights the unsteadiness of the compression waves and allows to identify their mean characteristic frequency which is around $1.5kHz$. This corresponds to a Strouhal number such as $S_L = fL/U_e = 0.12$. In the *initial part of the plateau zone* (see Figure 8(b)), no amplification can be observed whatever the frequency range downstream from the compression waves. In the *second part of the plateau zone* (see Figure 8(c)), a global amplification of perturbations is observed for frequencies ranging from $1kHz$ to $35kHz$ ($S_L \simeq 0.1$ to 3). These scales are amplified all along the interaction, with a maximum of amplitude around $f = 15kHz$ ($S_L = 1.5$). Another characteristic amplified frequency range can be observed on the figure : intermediate frequencies around $f = 5kHz$ ($S_L = 0.5$).

In our transitional interaction case, the Reynolds number at separation point is $Re_{X_0} = 365000$. Hot wire measurements inside the upstream laminar boundary layer exhibit so low level that growing of any characteristics times scales of the boundary layer was above measurement uncertainty. Nevertheless, for higher Reynolds number $Re_x > 900000$, Power Spectrum Density of laminar boundary layer perturbations highlights amplification of bandwidth frequency around $S_L = 1.5, f = 15$kHz. This suggest that the amplified modes in the interaction, around $S_L = 1.5$, have to be related to the unsteady modes of upstream laminar boundary layer.

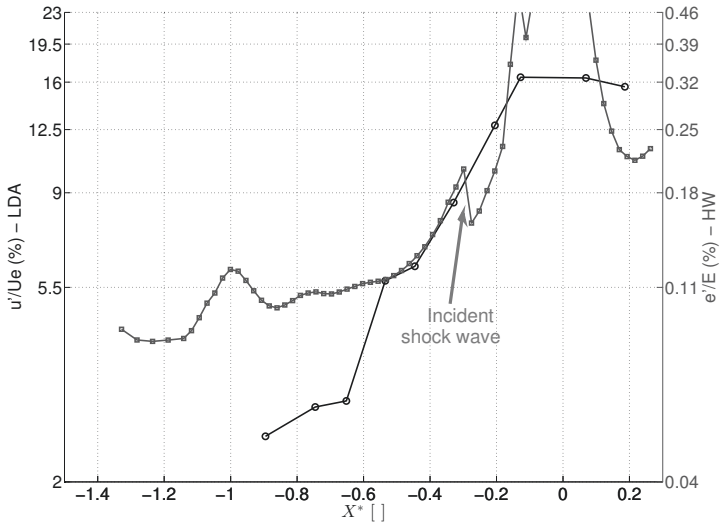

Figure 7: Broadband intensity of fluctuations, ($P_0 = 0.4atm$, $\theta = 5°$). ◯: LDA , local maxima; □Hot Wire, $y = 5mm$ from the wall.

5.0 TRANSITION MECHANISM

From the results presented in the previous section, we envisage to estimate the frequency response of the shock-induced separation subjected to a constant forcing defined by the upstream perturbations coming from the laminar boundary layer. Investigation of the frequency response of the interaction is here divided in three zones as defined earlier: *compression zone*, *first part of the plateau zone* and *second part of the plateau zone*.
On Figure 9, are plotted the transfer functions across each zone. This function is defined as the ratio between the PSD at a given measurement point and the PSD measured upstream from the compression waves. It characterizes the whole amplification or dumping of the fluctuations from the upstream of the interaction up to the measurement point.
Across the *compression zone*, we notice a relatively strong amplification of the voltage fluctuations energy at low frequencies.
Another trend is observed across the *first part of the plateau zone*: low frequencies energy ($< 1kHz$) are dumped, whereas the fluctuations at intermediate frequencies are slightly increased. In the compression zone, low frequency amplitudes have to be compared with the intermittent signal generated by the unsteady compression waves. Therefore, they have not to be compared with low frequency amplitudes of the radiated perturbations downstream from the compression waves.
Finally, we notice, across the whole *final part of the plateau zone*, an increase of the energy of all the characteristic frequency ranges ($S_L = 0.12$, 0.5 and 1.5) with an amplification ratio up to ten times higher compared to the upstream region.
An attempt was made to modeling the radiated pressure fluctuations measurements centered around $S_L = 1.5$. It is summarized Figure 10. It defines the measured Hot Wire signals as the superposition of two sources. The first one (horizontal black line) corresponds to the noise of the wind tunnel, mainly the pressure fluctuations radiated by the sidewalls turbulent boundary layers. It is considered as constant along X and estimated upstream from the SWBLI. The second one corresponds to the radiated pressure fluctuations from the interaction,

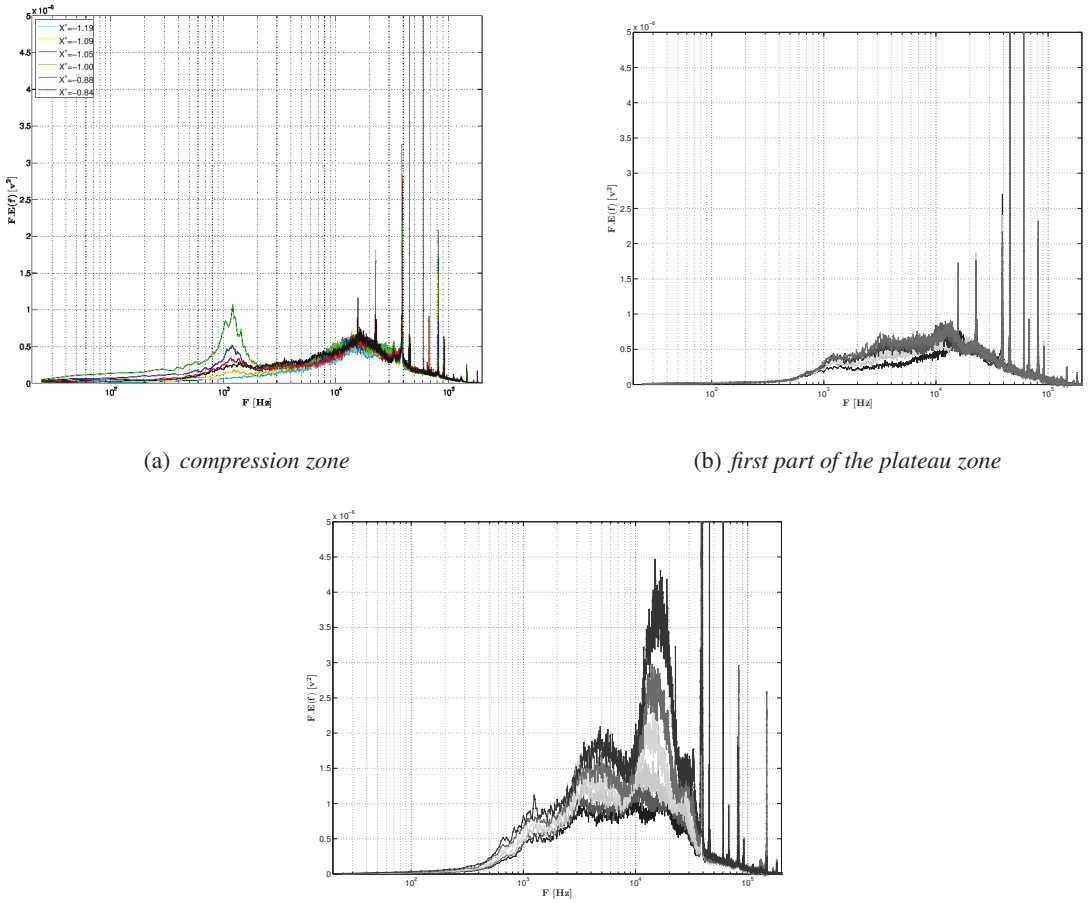

(a) *compression zone*

(b) *first part of the plateau zone*

(c) *second part of the plateau zone*

Figure 8: Premultiplied PSD through the interaction : $P_t = 0.4atm$, $\theta = 5°$, measurement at $y = 5mm$

centered around a Strouhal number of 1.5. They are increasing exponentially in the downstream direction, as suggested by the Figure 7. Two scenarii are considered:

- a constant growing rate of the fluctuations (G) along the interaction (dashed black line)
- a growing rate increasing continuously from 0 to G in the first part of the *plateau zone* and constant in the second part, as suggested Figure 9 (thin black line).

The initial level of the fluctuations and the growth rate G are adjusted with a best fit of the experimental results (thick black line): it corresponds to a growth rate G of $305m^{-1}$.
A global overview of the transition process along the interaction can be inferred from the present measurements. It is reported Figure 11. The upstream flow is a laminar boundary layer. At the separation point ($X^* = -1$), compression waves are developing and the decelerated shear layer is growing down to the apex location (around $X^* = -0.2$). The flow deviation at the separation point has been derived from mean external pressure measurements. It is less than the half of the imposed flow deviation as proposed in the Free Interaction Theory [6].

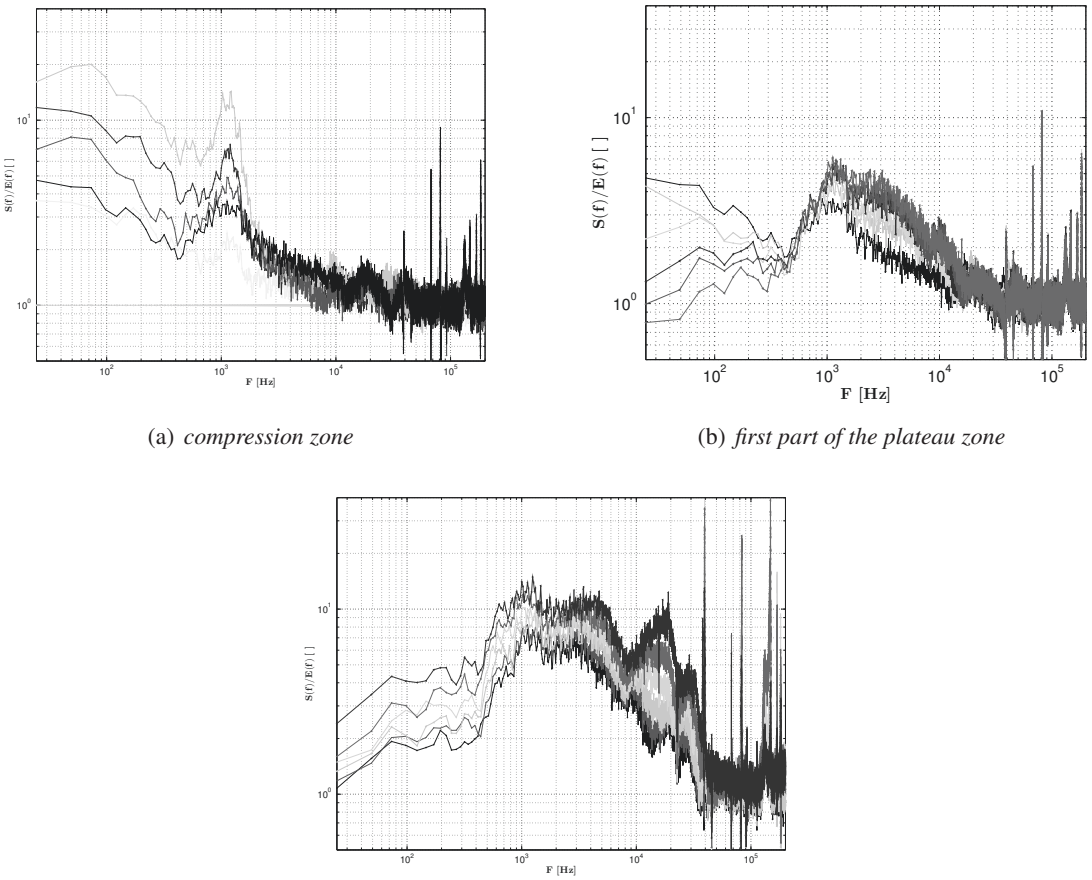

(a) *compression zone*

(b) *first part of the plateau zone*

(c) *second part of the plateau zone*

Figure 9: Transfer functions through the interaction : $P_t = 0.4atm$, $\theta = 6°$, measurement at $y = 5mm$

In the upstream laminar boundary layer, unsteady modes are developing, with very low amplitude for such Reynolds number ($Re_{X_0} = 365000$). These modes correspond to high frequencies (about 15kHz, $S_L = 1.5$ in our case). They are strongly amplified (mainly in the second part of the *plateau zone*) along the separated shear layer, with an exponential growth, up to a saturation level which corresponds to transitional-turbulent values. This increase dramatically the momentum transfer across the shear layer and the flow is reattaching. The large scales developed along the interaction are shed downstream from the reattachment. This is similar to results of [10] who forced a separated interaction with unstable modes of the separated bubble obtained by Linear Stability Theory (LST) and found these unstable modes to experience a weak growth along the attached boundary layer and a strong growth inside the bubble that may lead to a non-linear interaction and then to turbulence break-down. Therefore, it seems that, for this range of frequencies, the transitional SWBLI can be considered as a noise amplifier.

The downstream boundary layer is out of equilibrium, with maxima of velocity fluctuations larger than in undisturbed boundary layer. This is very similar to what is observed in separated turbulent shock wave boundary layer interactions, despite significant differences between the Strouhal number (0.5 and 1.5 respectively for the

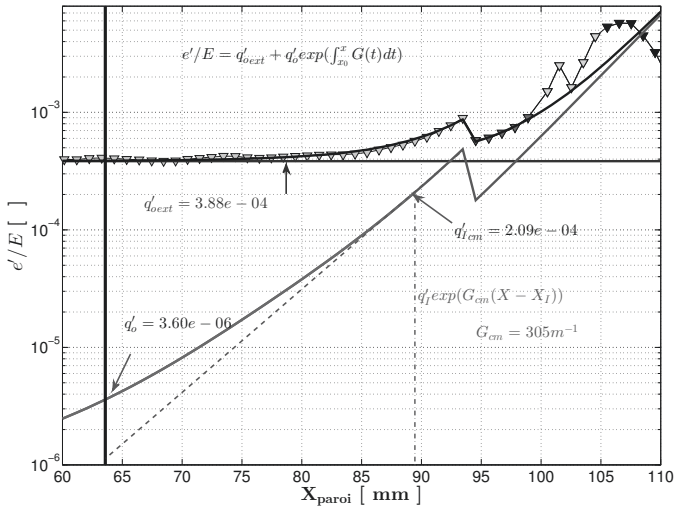

Figure 10: Modeling of the growth of the upstream perturbations along the separated shear layer. Symbols: experiments; lines: model.

turbulent and transitional cases).
Over imposed on these high frequency unsteadiness, very low frequencies are observed all along the interaction. They correspond to dimensionless frequencies around $S_L = 0.12$ and are clearly associated with low frequency motions of the initial compression waves. This value differs significantly from the dimensionless low frequencies associated to separated shock of turbulent interactions, which is around $S_L = 0.03$. In [13], it was suggested that the low frequency unsteadiness in SWBLI should vary as the aspect ratio l/h of the separated bubble. The aspect ratio of transitional and turbulent SWBLI can be approximated from the flow deviation θ_{sep} at the separation point: $l/h \simeq 1/tan(\theta_{sep})$. In our transitional interaction configuration, a flow deviation angle of 2° has been obtained, against around 10° flow deviation angle for turbulent SWBLI ([21]). Then a ratio of about $(l/h)_{tr}/(l/h)_{turb} = tan(10)/tan(2)$ can be expected between the low frequency transitional and turbulent Strouhal numbers. Thus, the dimensionless low frequency of SWBLI for turbulent and laminar cases should be related as $(S_L)_{tr} = tan(10)/tan(2) \times (S_L)_{turb} = 0.15$. The expected Strouhal number is approximatively equal to the one found in our configuration. Therefore, present measurements seem to confirm the low frequency dependence on the aspect ratio of the interaction.
Otherwise, perturbations through the interaction exhibit a medium frequency around $S_L = 0.5, f = 5$kHz which is amplified along the interaction. The same Strouhal number have been found in turbulent SWBLI, and has been related to convective structures developing along the shear layer with convective velocity of $U_c/U_e \simeq 0.3$ and characteristic wavelengths as $\lambda/L \simeq 0.6$, [22]. Nevertheless, the very large aspect ratios in transitional cases suggest that such assumption is not more relevant, as such unsteadiness would involve wavelength of about 100 initial boundary layer displacement thickness. Therefore, additional elements, as phase velocity, are clearly required to analyze these intermediate time scales.

6.0 CONCLUSION

We considered a transitional SWBLI at free Mach number 1.68 and moderate unit Reynolds numbers. The aspect ratio of the separation is much higher in the transitional interaction ($L/\delta_o^* = 159$) than in the turbulent

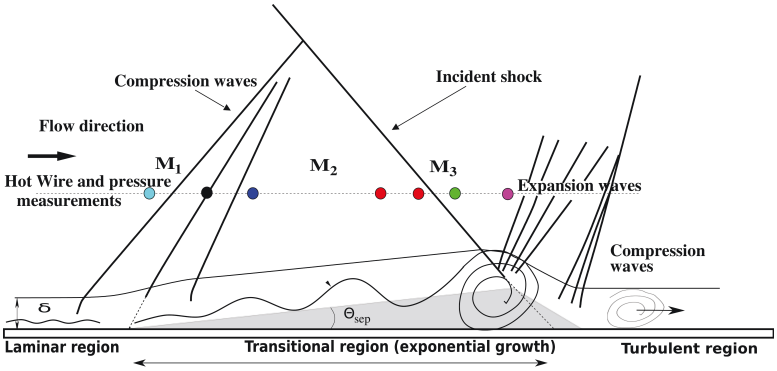

Figure 11: Sketch of the transition development along the interaction.

one. A model to evaluate the accuracy limitation of the LDA data, taking into account the size of the probe volume with respect to the boundary layer thickness, has been proposed. A specific LDA set-up has been defined. It allows to reduce the apparent velocity fluctuations due to the finite size of the probe volume in respect with the local velocity gradient. Perturbations along the separated shear layer are found to increase exponentially, and may be responsible for laminar-turbulent transition that takes place inside the bubble. Hot wire measurements of the pressure fluctuations radiated from the shear layer show that this transition process results from the contribution of several bandwidth frequencies. The high frequencies correspond to a strong amplification along the separated shear layer of the upstream perturbations which are developing in the upstream laminar boundary layer. They are amplified up to a saturation level which defines the transition to turbulence of the flow: at this station, the flow is reattaching. For this range of frequencies, the interaction can be considered as a noise amplifier.
Superimposed are low and intermediate frequencies. The low ones are associated with the low frequency breathing of the interaction and can be compared with classical results in turbulent separated SWBLI if the differences between transitional and turbulent aspect ratio are considered. Intermediate frequencies are still to be describe and need further analysis.

ACKNOWLEDGMENTS

This work received financial support by the TFAST Project of the European Commission's 7th Framework Programme 265455 and the Labex MEC. These supports are gratefully acknowledged.

REFERENCES

[1] Gadd, G. E. H. D. W. R. J. D., "An experimental investigation of the interaction between shock waves and boundary layers," 1954.

[2] Hakkinen, R., Greber, I., and Trilling, L., "The interaction of an oblique shock wave with a laminar boundary layer," Tech. rep., mar 1959.

[3] Katzer, E., "On the lengthscales of laminar shock/boundary-layer interaction," *J . Fluid Mech*, Vol. 206, 1989, pp. 477–496.

[4] Mallinson, S. G., Gai, S. L., and Mudford, N. R., "The interaction of a shock wave with a laminar boundary layer at a compression corner in high-enthalpy flows including real gas effects." *J . Fluid Mech*, Vol. 342, 1997, pp. 1–35.

[5] Chanetz, B., Benay, R., Bousquet, J.-M., Bur, R., Pot, T., Grasso, F., and Moss, J., "Experimental and numerical study of the laminar separation in hypersonic flow," *Aerospace Science and Technology*, , No. 3, 1998, pp. 205–218.

[6] Chapman, D. R., Kuehn, D. M., and Larson, H. K., "Investigation of separated flow in supersonic and subsonic streams with emphasis of the effect of transition," Tech. rep., 1957.

[7] Giepman, R., *Flow Control for Oblique Shock Wave Reflections*, Ph.D. thesis, Delft University of Technology.

[8] Bur, R. and Garnier, E., "36th month Work Progress Report," Tech. Rep. 36th month, ONERA, March 2015.

[9] Sansica, A., Sandham, N. D., and Hu, Z., "Forced response of a laminar shoc-induced separation bubble," *Physics of Fluids*, , No. 26, 2014.

[10] Sansica, A., Sandham, N. D., and Hu, Z., "Instability and low-frequency unsteadiness in a shock-induced laminar separation bubble," *J. Fluid Mech.*, Vol. 798, May 2016, pp. 5–26.

[11] Larchevêque, L., "Low and Medium Frequency Unsteadinesses in a Transitional Shock-Boundary Reflection with Separation," *54th AIAA Aerospace Sciences Meeting*, 2016.

[12] Giepman, R. H. M., F. F. J., S., and Oudheusden, B. W., "High resolution PIV measurements of a transitional shock wave boundary layer interaction ," *Experiments in Fluids*, Vol. 56, April 2015.

[13] Piponniau, S., Dussauge, J. P., Debiève, J. F., and Dupont, P., "A simple model for low-frequency unsteadiness in shock-induced separation," *Journal of Fluid Mechanics*, Vol. 629, 2009, pp. 87–108.

[14] Diop, M., Piponniau, S., and Pierre, D., "On the length and time scales of a laminar shock wave boundary layer interaction," *54th AIAA Aerospace Sciences Meeting*, American Institute of Aeronautics and Astronautics, 2016/02/18 2016.

[15] Durst, F., Melling, A., and Whitelaw, J., *Principles and Practice of Laser-Doppler Anemometry*, 1976.

[16] Diop, M., Piponniau, S., and Dupont, P., "Transition mechanism in a shock wave boundary layer interaction," *Tenth International Symposium on Turbulence and Shear Flow Phenomena 2017*, 2017.

[17] Agostini, L., Larchevêque, L., Dupont, P., Debiève, J., and Dussauge, J., "Zones of influence and shock motion in a shock boundary layer interaction," *AIAA Journal*, Vol. 50, No. -6, june 2012, pp. 1377–1387.

[18] Délery, J. M. and Marvin, J. G., "Shock wave - boundary layer interactions," Tech. rep., 1986.

[19] Smits, A. J. and Dussauge, J. P., *Turbulent shear layers in supersonic flow*, AIP Press, 2nd ed., 2006.

[20] Jaunet, V., Debiève, J. F., and Dupont, P., "Length Scales and Time Scales of a Heated Shock-Wave/Boundary-Layer Interaction," *AIAA Journal*, 2014/08/30 2014, pp. 1–9.

[21] Green, J., "Reflexion of an oblique shock wave by a turbulent boundary layer," *Journal of Fluid Mechanics*, Vol. 40, 1970, pp. 81–95.

[22] Dupont, P., Haddad, C., and Debiève, J. F., "Space and time organization in a shock induced boundary layer," *Journal of Fluid Mechanics*, Vol. 559, 2006, pp. 255–277.